quantum reports

IMPACT FACTOR 1.3

CITESCORE 3.0

Article

Simulating Methylamine Using a Symmetry-Adapted, Qubit Excitation-Based Variational Quantum Eigensolver

Konstantin M. Makushin and Aleksey K. Fedorov

MDPI

https://doi.org/10.3390/quantum7020021

quantum reports

MDPI

Article

Simulating Methylamine Using a Symmetry-Adapted, Qubit Excitation-Based Variational Quantum Eigensolver

Konstantin M. Makushin [1,*] and Aleksey K. Fedorov [2]

[1] Department of Theoretical Physics, Institute of Physics, Kazan Federal University, Kazan 420008, Russia
[2] National University of Science and Technology "MISIS", Moscow 119049, Russia; fedorov.ak@misis.ru
* Correspondence: llconstantinel@gmail.com

Abstract: Understanding the capabilities of quantum computer devices and computing the required resources to solve realistic tasks remain critical challenges associated with achieving useful quantum computational advantage. We present a study aimed at reducing the quantum resource overhead in quantum chemistry simulations using the variational quantum eigensolver (VQE). Our approach achieves up to a two-orders-of magnitude reduction in the required number of two-qubit operations for variational problem-inspired ansatzes. We propose and analyze optimization strategies that combine various methods, including molecular point-group symmetries, compact excitation circuits, different types of excitation sets, and qubit tapering. To validate the compatibility and accuracy of these strategies, we first test them on small molecules such as LiH and BeH_2, then apply the most efficient ones to restricted active-space simulations of methylamine. We complete our analysis by computing the resources required for full-valence, active-space simulations of methylamine (26 qubits) and formic acid (28 qubits) molecules. Our best-performing optimization strategy reduces the two-qubit gate count for methylamine from approximately 600,000 to about 12,000 and yields a similar order-of-magnitude improvement for formic acid. This resource analysis represents a valuable step towards the practical use of quantum computers and the development of better methods for optimizing computing resources.

Keywords: quantum computing; quantum chemistry; variational algorithms; vqe; variational ansatz

Received: 24 March 2025
Revised: 17 April 2025
Accepted: 19 April 2025
Published: 21 April 2025

Citation: Makushin, K.M.; Fedorov, A.K. Simulating Methylamine Using a Symmetry-Adapted, Qubit Excitation-Based Variational Quantum Eigensolver. *Quantum Rep.* **2025**, *7*, 21. https://doi.org/10.3390/quantum7020021

1. Introduction

An accurate description of the electronic structure of molecular ground and excited states is fundamental to progress in areas such as catalysis and the design of functional materials [1]. However, the computational complexity of exact quantum chemistry simulations for many relevant situations grows exponentially with the system size [2]. This problem has stimulated the development of classical approaches that capture relevant chemical properties [3], yet the simplifications used in such approaches may hinder underlying electronic correlation effects that can play an important role in various systems.

To overcome these limitations and address the problem of growing computational demands, the quantum computing paradigm presents a promising solution [4–6]. By leveraging the principles of quantum physics, quantum computing devices offer the potential to efficiently solve complex quantum–chemical problems that are intractable for classical computers [5,6].

In this context, several quantum hardware paradigms have been explored for quantum chemistry applications. First, special-purpose quantum devices can be used [7]. In particular, boson sampling [8], analog quantum simulators [9], and quantum annealing

devices [10] have been used to solve various chemical problems; however, the encoding of chemical problems into the setting of special-purpose quantum computers may hinder the potential quantum computational advantage [11,12]. Second, universal quantum computing models—specifically, gate-based quantum computers—have the potential to be used for quantum chemistry simulations [4–6]. In order to encode electronic states of molecules into qubits, one uses a basis of predefined spin orbitals, i.e., quantum states that can be occupied by individual electrons. Each qubit in the quantum register represents one such spin orbital, with its value (0 or 1) determining whether this spin orbital is occupied or not. The molecular state is then a superposition of multiple occupancy configurations. A quantum computing device is then used, e.g., to find the lowest energy state of molecules.

However, a full quantum simulation using gate-based quantum computers requires prohibitively large amounts of resources—specifically, the number of two-qubit operations [5,6]. The ability to implement two-qubit operations in existing quantum computing devices is limited by the amount of errors due to the effects related to interactions with the environment. In this context, the variational quantum eigensolver (VQE) approach [13–16] is of interest, since this algorithm can be implemented with the use of existing noisy intermediate-scale quantum (NISQ) devices. VQE has shown its ability to calculate molecular ground states and energy spectra with chemical accuracy in a number of studies [7,15–17].

In this work, we analyze the resources that are required to simulate certain molecules on a medium-scale quantum computer with the use of the VQE approach, taking into account possible optimization. Specifically, we combine the use of molecular point-group symmetries (symmetry adaptation), compact excitation circuits (qubit excitation-based), several types of excitation sets, and the qubit tapering method. As we demonstrate, these optimizations allow for a significant reduction in computational requirements while ensuring convergence to the required energies. First, we apply these combinations to small molecules, such as LiH and BeH_2, to evaluate their compatibility, accuracy, and potential applicability to larger problems. We then simulate the methylamine molecule within its restricted active space using the best-performing optimization strategies. Finally, we complete our analysis by computing the resources required for full-valence, active-space simulations of methylamine and formic acid molecules, which, using our best optimization strategy, would require around 10,000–15,000 two-qubit gates. Both the two-qubit gate count and circuit depth are improved by nearly two orders of magnitude compared to the naive approach. Our results demonstrate that these optimization strategies perform well and can make such simulations more feasible for near-term quantum computers.

The paper is organized as follows. In Section 2, we formulate the VQE approach to solve quantum–chemical problems. In Section 3, we review recent related studies. In Section 4, we take into account possible optimization techniques that can be used to reduce the computational cost of VQE-based quantum–chemical simulations. Our results are summarized in Section 5, alongside an analysis of the quantum resources required to simulate methylamine and formic acid molecules. In Section 6, we analyze the reasons for the efficiency of our proposed optimization strategies. Conclusions are presented in Section 7.

2. VQE Formalism

During the last decade, a large variety of modifications of the VQE approach have been proposed [15], the majority of which are based on the Ritz variational principle. The Ritz principle involves choosing a certain parameterized combination of wave functions or state vectors, i.e., the ansatz, and minimizing the functional defined on this parameterized combination. Choosing the right ansatz should take into account the specifics of the problem

and its boundary conditions. In other words, the ansatz represents a linear combination of some known functions, which are parameterized by some unknown coefficients:

$$\Psi = \sum_i \theta_i \psi_i. \tag{1}$$

Let $\mathcal{H}$ be the Hamiltonian of a certain physical system, with its spectrum of eigenvalues bounded from below by the minimum eigenvalue (E_0). Assuming that the state vector ($|\Psi\rangle$) can be described using a set of variable parameters ($\boldsymbol{\theta} = \{\theta_1, \theta_2, \ldots, \theta_i\}$) similarly to Equation (1), we can approximate the ground-state energy of the Hamiltonian by minimizing the following functional, which is expressed with the following inequality:

$$E_0 \leq \frac{\langle \Psi(\boldsymbol{\theta}) | \mathcal{H} | \Psi(\boldsymbol{\theta}) \rangle}{\langle \Psi(\boldsymbol{\theta}) | \Psi(\boldsymbol{\theta}) \rangle}. \tag{2}$$

The ansatz always gives an expected value that is greater than or equal to the ground-state energy. However, if the chosen ansatz is a wave function orthogonal to the ground-state wave function, then this method would give an estimate for one of the excited states of the system.

The general idea behind all VQE-type algorithms boils down to the following. As a first step, it is necessary to define a target function (C) that encodes the solution to the problem. Then, one has to choose a suitable ansatz depending on a discrete or continuous set of parameters ($\boldsymbol{\theta}$). After that, one needs to perform optimization of the target cost function using a classical computer:

$$\boldsymbol{\theta}^* = \arg\min_{\boldsymbol{\theta}} C(\boldsymbol{\theta}) \tag{3}$$

Considering the molecular ground-state estimation problem, it is necessary to map the molecular Hamiltonian to the qubit Hamiltonian. Under the Born–Oppenheimer approximation, the molecular Hamiltonian is usually expressed in its second quantized form:

$$H = \sum_{p,q=1}^{M} h_{pq} a_p^\dagger a_q + \frac{1}{2} \sum_{p,q,r,s=1}^{M} g_{pqrs} a_p^\dagger a_r^\dagger a_s a_q, \tag{4}$$

where $a_p^\dagger (a_p)$ is the fermionic creation (annihilation) operator and M is the total number of spin orbitals. Coefficients h_{pq} and g_{pqrs} are called one- and two-electron integrals, respectively, and can be computed classically.

To transform fermionic operators into qubit operators, several mappings, such as Jordan–Wigner, parity, and Bravyi–Kitaev mappings, can be used. After the transformation is realized, one obtains a qubit Hamiltonian in the following form:

$$H = \sum_i \beta_i P_i, \quad \text{with} \quad P_i = \bigotimes_{k=1}^{N} \sigma_k^{(i)}, \tag{5}$$

where each $\sigma_k^{(i)} \in \{I, X, Y, Z\}$ is a Pauli operator, N is the number of qubits, and P_i are Pauli strings. Each Pauli string can then be measured individually or in commutative groups using additional post-rotation gates, preceded by the same ansatz circuit for every Pauli string.

The parameterized ansatz can be chosen based on a completely heuristic approach or on physical intuition. In the case of quantum chemistry, we can adopt the well-known Unitary Coupled Cluster (UCC) ansatz, which can recover a portion of the electron correlation

energy by evolving the Hartree–Fock initial wave function. Using the Hartree-Fock state as a reference, we can write the following expression:

$$|\Psi(\boldsymbol{\theta})\rangle = \hat{U}(\boldsymbol{\theta})|\psi_{HF}\rangle = e^{\hat{T}(\boldsymbol{\theta})-\hat{T}^{\dagger}(\boldsymbol{\theta})}|\psi_{HF}\rangle, \tag{6}$$

where $\hat{T}(\boldsymbol{\theta})$ is a parameterized cluster operator and $\hat{U}(\boldsymbol{\theta})$ represents the corresponding unitary ansatz. Usually, only single-electron and double-electron excitations are considered, so

$$\hat{T}(\boldsymbol{\theta}) = \hat{T}_1(\boldsymbol{\theta}) + \hat{T}_2(\boldsymbol{\theta}) = \sum_i \theta_i P_i. \tag{7}$$

The algorithm for the classical optimization part of VQE should be chosen based on the specifics of the convergence, resource requirements, and noise tolerance for a certain problem. For instance, gradient-based optimizers like BFGS and L-BFGS are often preferred for smooth parameter landscapes due to their fast convergence [18], while derivative-free methods such as Constrained Optimization BY Linear Approximations (COBYLA) [19] and Simultaneous Perturbation Stochastic Approximation (SPSA) [20] may better handle noisy quantum hardware at the cost of increased circuit evaluations. Additionally, the choice must balance computational overhead with the scale of the problem, as iterative algorithms such as Adaptive Moment Estimation (ADAM) [15] can adaptively adjust learning rates but may struggle with high-dimensional parameter spaces typical in large molecular systems.

3. Related Work

While Section 1 outlines the broader motivation for quantum computing in chemistry, here, we focus on the on recent advances that have shaped VQE-based methods and related hybrid quantum algorithms.

Variational approaches based on VQE have been used to analyze small molecules such as hydrogen (H_2) [18,21,22], lithium hydride (LiH) [22], beryllium hydride (BeH_2) [18], and water (H_2O) [23], as well as to simulate diazene isomerization [24] and carbon monoxide oxidation [16]. An overview of the VQE developments, showcasing its adaptability and potential for complex quantum systems, is presented in Ref. [7]. For example, a recent study [17] highlighted methodological advancements and best practices in applying VQE to quantum chemistry problems, emphasizing its versatility for a variety of molecular systems. VQE has also been used in benchmarking studies with different hardware platforms and molecular configurations [25,26] and in specialized tasks such as sophisticated Hamiltonian corrections for molecular simulations and the computation of magnetic properties of rare-earth ions [27,28].

Making VQE tractable on near-term hardware typically involves circuit depth optimization, error mitigation, or factorization-based resource reduction [29,30]. Large-scale implementations of VQE on high-performance supercomputers, which highlight the method's scalability for difficult systems, were studied in Ref. [31]. All of this research supports the idea that VQE is an attractive option for addressing quantum–chemical challenges beyond the capabilities of classical computing, givenfurther algorithmic improvements and better quantum hardware. Meanwhile, broader families of variational hybrid algorithms go beyond quantum chemistry. Examples include the quantum approximate optimization algorithm (QAOA) [32–34], which targets combinatorial optimization tasks, and the variational spin-squeezing algorithm (VSSA) [35–37], focusing on generating spin-squeezed states for metrological applications. Recently, there has been growing interest in combining machine learning strategies with both classical and quantum algorithms. In the classical domain, robust local–global modeling and domain-adaptation techniques have been proposed to handle uncertain or noisy data [38,39]. At the same time, in quantum

computing, machine learning-based methods have been explored for the acceleration of VQE optimization and the enhancement of ansatz expressiveness. For instance, neural network ansatzes have shown promise as a flexible representation of many-electron wave functions [40–42], paving the way for more compact and efficient VQE simulations on near-term quantum hardware.

Alternative methods for constructing the variational ansatz, such as the use of adaptive ansatzes [16,43] or evolutionary algorithms [44], aim to reduce computational overhead by incrementally building the circuit. In the adaptive approach, excitation operators are selected one by one based on their energy-gradient contributions, allowing the ansatz to grow in a problem-specific and compact manner.

Collectively, these lines of research—from small-molecule studies and benchmark tasks to circuit optimization, adaptive ansatz construction, and machine learning-based strategies—highlight the growing sophistication of VQE-based methods and their expanding potential to address larger and more complex chemical systems on near-term quantum hardware.

4. Molecular Setup and Optimization Techniques

In this section, we describe the molecular systems under study and outline the optimization techniques employed to reduce the quantum resource requirements for their simulation within the VQE framework.

Methylamine (CH_3NH_2) and formic acid (CH_2O_2), also known as methanoic acid, are both simple yet fundamental organic compounds in chemistry and biochemistry. Methylamine, an amine related to ammonia, is crucial in manufacturing pesticides, pharmaceuticals, and solvents and constitutes an amino acid, which are building blocks of protein [45]. Formic acid, the simplest carboxylic acid, is found in insect stings and is utilized industrially in making leather and textiles and as a feed preservative. Both play significant roles in biological systems [46], with formic acid also acting as a key metabolic agent and a strong solvent. More precise understanding of their properties and the features of compounds on their basis may provide valuable information for various problems in chemistry and life sciences. We now turn to evaluating the quantum resources required to simulate these molecules.

As discussed in Section 2, considering fermionic transformations and the minimal Slater-type orbital basis set with three Gaussians (STO-3G), each spin orbital can be encoded with one qubit. Thus, the total number of qubits is equal to the number of spin orbitals: $N_q = M$. For formic acid and methylamine, we have 17 and 15 molecular orbitals correspond to 34 and 30 spin orbitals, respectively, and, thus, to the number of qubits required for each system. The number of qubits can be reduced by employing the frozen core approximation, where the inner 1s orbitals of carbon and oxygen in the formic acid molecule and carbon and nitrogen in the methylamine molecule are kept frozen. This step reduces the required number of qubits by six for formic acid and by four for methylamine.

Additionally, by applying a technique known as *qubit tapering* [47], one can exploit symmetries of the system to find a unitary transformation (U) that acts on the Hamiltonian (5) such that

$$H' = UHU^\dagger = \sum_i \beta'_i P'_i, \tag{8}$$

where H' has the same eigenvalues as H. After this transformation, there are operators acting trivially in each Pauli string (P'_i) of the transformed Hamiltonian. In other words, the Pauli strings have either the identity operator (I) or the same Pauli operator (e.g., X) at specific qubit positions across all H' terms. These operators can be replaced by their eigenvalues, and the corresponding qubits can be effectively removed from the simulation.

In general, if there are m independent $\mathbb{Z}_2$ symmetries, the number of active qubits is reduced by m. In the case of formic acid and methylamine molecules, we can eliminate three additional qubits from our simulation for both molecules, resulting in final qubit counts of 25 and 23, respectively.

Table 1. Calculated atomic coordinates for methylamine (CH_3NH_2) and formic acid (CH_2O_2) in angstroms. The coordinates are sourced from the CCCBDB database [48] and optimized at the CCSD(T) level of theory with the Def2TZVPP basis set.

Molecule	Atom	X (A)	Y (A)	Z (A)
Methylamine	C	0.0519020	0.7064670	0.0000000
	N	0.0519020	−0.7615000	0.0000000
	H	−0.9428060	1.1684160	0.0000000
	H	0.5906740	1.0624810	0.8789330
	H	0.5906740	1.0624810	−0.8789330
	H	−0.4566340	−1.1008410	−0.8075530
	H	−0.4566340	−1.1008410	0.8075530
Formic Acid	C	0.0000000	0.3858930	0.0000000
	O	−0.8988900	−0.6261750	0.0000000
	O	1.1799510	0.1951720	0.0000000
	H	−0.4628290	1.3844990	0.0000000
	H	−1.7856570	−0.2518330	0.0000000

Utilizing the coordinates in Table 1 allows us to derive the qubit form of the molecular Hamiltonian (5) and ascertain the number of terms it contains. For molecular Hamiltonians, it scales with the number of electrons (N) as $\mathcal{O}(N^4)$. This plays a central role in defining the required number of quantum circuits to be measured at each iteration and represents one of the major bottlenecks in VQE implementation for complex molecules. To partially overcome this problem, one can adopt more sophisticated grouping methods for Pauli terms, such as *qubit-wise* and *general* methods. These methods use the commutative properties of Pauli terms to notably decrease the number of necessary measurements, scaling as $\sim \mathcal{O}(N^4/30)$ for large Hamiltonians. We can say that two Pauli strings commute *qubit-wise* if, at each index, the corresponding two Pauli operators commute, for instance, Pauli strings like $\{YY, YI, IY, II\}$. In the case of *general* commutativity, two Pauli strings commute if and only if they do not commute on an even number of indices, for example, $\{XX, YY, ZZ\}$ [49]. Such sets can be measured simultaneously with a single circuit, leveraging their commutativity.

In considering the Unitary Coupled-Cluster Singles and Doubles (UCCSD) variational ansatz and employing first-order Suzuki–Trotter decomposition, we aim to quantify the number of electronic excitations, the depth of the parameterized quantum circuit, and the total number of gates within these circuits. If we consider a system with N electrons and define the number of single excitations as $N_S = N(M-N)$ and the number of double excitations as

$$N_D = \frac{N(N-1)}{2}\,\frac{(M-N)(M-N-1)}{2}, \tag{9}$$

then the total number of one-qubit and two-qubit gates in the ansatz circuit can be approximately estimated as follows:

$$\begin{aligned} N_{\text{1-qubit}} &= \alpha_S\, N_S + \alpha_D\, N_D, \\ N_{\text{2-qubit}} &= \beta_S\, N_S + \beta_D\, N_D. \end{aligned} \tag{10}$$

where α_S (β_S) is the average number of one-qubit (two-qubit) gates per single excitation and α_D (β_D) is the average number of one-qubit (two-qubit) gates per double excitation.

The total circuit depth can be estimated in a similar way:

$$d = \gamma_S N_S + \gamma_D N_D, \tag{11}$$

where γ_S and γ_D are the contributions to the circuit depth from single and double excitations, respectively. The coefficients from Equations (10) and (11) depend on the actual definition of excitation sub-circuits in the ansatz, the fermionic transformation used, and the number of qubits. Standard implementations of Pauli string exponentials (6) and (7) in quantum circuits typically rely on sequences of single-qubit rotations and cascades of two-qubit CNOT-gates (or CX-gates) arranged in a ladder-like structure. Recent papers have presented optimal ways of constructing such circuits with fewer entangling operations [50–52]. One approach is to use qubit excitations, which always require a fixed number of these gates. However, it remains unclear whether they can adequately account for the electronic correlation contribution, as they ignore the anticommutation of fermions by excluding Pauli Z products from the operator exponent.

A naive implementation of the UCCSD ansatz leads to excessive resource requirements because the circuit depth (11) is proportional to the number of double excitation operators, which scales as $\mathcal{O}(N^4)$. However, one can employ several techniques to reduce the number of these operators. One of them is the k-UpCCGSD (for brevity, k-UpGSD) [53,54] ansatz, where k represents the number of ansatz repetitions, each with a new set of variational parameters; p refers to paired excitations; and G denotes the inclusion of generalized excitations. The main difference from UCCSD is that it includes only two-body terms, which shift pairs of opposite-spin electrons from fully occupied to completely unoccupied spatial orbitals, making sure there are no singly occupied states described. The depth of the ansatz circuit can be reduced because the number of paired generalized excitations is typically significantly smaller than the number of double excitation operators in standard UCCSD, which are the primary contributors to circuit depth.

Another way to optimize the number of operators in the UCCSD ansatz is to filter out the excitations based on their irreducible representations [55]. In other words, one should retain only those operators whose irreducible representations coincide with the irreducible representation of the initial state (Hartree–Fock determinant). In the case of doubly occupied molecular orbitals we can write the following:

$$\forall \Gamma \left(e^{\hat{T}-\hat{T}^\dagger} |\psi_{HF}\rangle \right) = \Gamma(|\psi_{HF}\rangle) : e^{\hat{T}-\hat{T}^\dagger} = 1, \tag{12}$$

where Γ denotes the irreducible representation of the corresponding wave function, ensuring that only excitations preserving the symmetry of the reference state ($|\psi_{HF}\rangle$) are valid in the UCCSD ansatz.

Leveraging these methods, we now apply their various combinations in constructing parameterized quantum circuits for several molecules and analyze their impact on quantum resource requirements.

5. Results

We begin with two components: (1) qubit excitations (denoted as “Q”) and (2) irreducible representation filtering (denoted as “s”). These are combined with the UCCSD and k-UpGSD ansatzes to create hybrid UCCSDQ, UCCSDQs, and k-UpGSDQ ansatzes (see Figure 1).

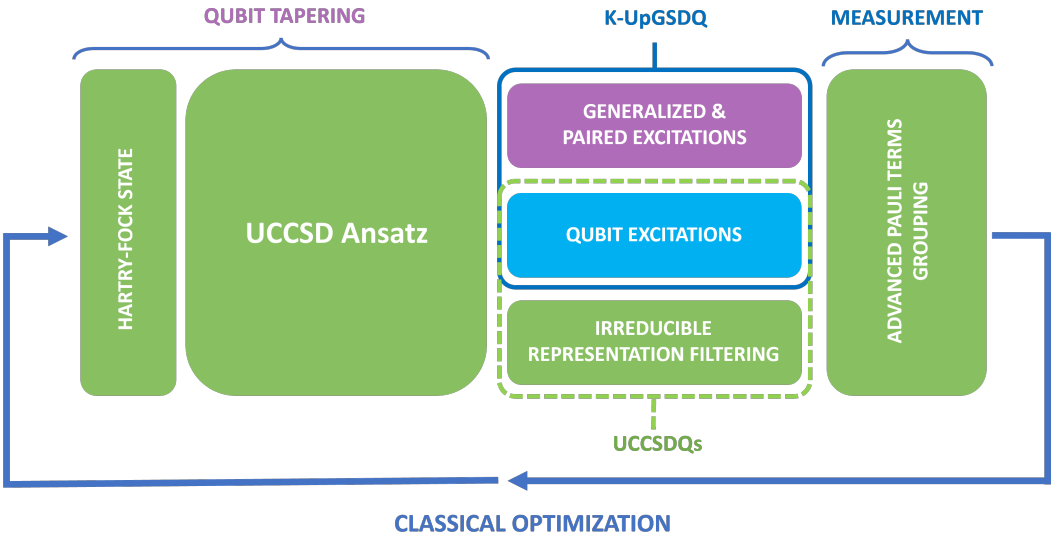

Figure 1. Hybrid quantum–classical VQE workflow used in this work. The diagram highlights the optimization techniques deployed and how they are combined. The green dashed box represents the methods used in the UCCSDQ ansatz, while the blue box corresponds to the k-UpGSDQ ansatz.

Additionally, we estimate the resources required for UCCSD and k-UpGSD ansatzes in combination with qubit tapering and compare the results with those of other optimization strategies. In all estimates, we use *qubit-wise* grouping of Pauli strings and a quantum chemistry library developed in-house for the efficient implementation of variational quantum algorithms [56].

Table 2. Estimated resources for the VQE computation of CH_3NH_2 and CH_2O_2 molecules. The number of qubits is calculated using the frozen core approximation and the qubit tapering procedure. The number of circuits is based on qubit-wise operator grouping. The parameters for the k-UpGSD and k-UpGSDQ ansatzes are estimated with $k = 1$. To obtain estimates for higher values of k, the table values should be multiplied by the corresponding scaling factor. The best-performing method in terms of the trade-off between required resources and VQE convergence to the FCI energy is highlighted in bold.

		CH_3NH_2		
Parameter	**UCCSD**	**k-UpGSD**	**UCCSDQs**	**k-UpGSDQ**
Circuit depth	514,379	14,758	**5766**	473
Qubits	23	23	**26**	26
Total gates	631,022	18,526	**11,558**	2822
Two-qubit gates	457,800	12,896	**4130**	1014
Pauli terms	20,908	20,908	**20,908**	20,908
Circuits	4144	4144	**4144**	4144
Double excitations	2394	78	**314**	78
Tapering	Yes	Yes	**No**	No
		CH_2O_2		
Circuit depth	563,722	15,026	**7563**	514
Qubits	25	25	**28**	28
Total gates	682,524	19,466	**14,610**	3294
Two-qubit gates	510,426	13,520	**5221**	1183
Pauli terms	30,423	30,423	**30,423**	30,423
Circuits	5103	5103	**5103**	5103
Double excitations	2745	91	**397**	91
Tapering	Yes	Yes	**No**	No

To verify that the chosen ansatz construction methods and optimization strategies work as expected, we test them on two relatively simple molecules, LiH and BeH_2, both with a small number of spin orbitals. The minimal STO-3G basis is employed for both molecules. For LiH, we consider freezing the inner 1*s* orbital, which results in 10 qubits in the non-tapered regime and 6 in the tapered regime. For BeH_2, we initially have 14 qubits. The frozen core method reduces this to 12 qubits in the non-tapered regime and 7 qubits with tapering. We then compute their ground-state energies using the VQE algorithm combined with the proposed optimization strategies. For both molecules, we use a noiseless state vector simulator in combination with the BFGS algorithm for classical optimization and Jordan–Wigner fermionic transformation.

The results of the VQE calculations for the LiH molecule are presented in Figure 2. The plot shows how the energy converges over iterations for various ansatz types, such as UCCSD and its generalized version, UCCGSD; 2-UpGSD; 2-UpGSDQ; UCCSDQ; and UCCSDQs. The dashed black line represents the exact Full Configuration Interaction (FCI) energy, which we use as a reference. The shaded area around it shows the chemical accuracy threshold of ± 0.0016 Hartree. Among all the ansatz types, UCCSDQs demonstrates the best performance: it achieves the lowest circuit depth (137) and two-qubit gate count (86) while still maintaining chemical accuracy.

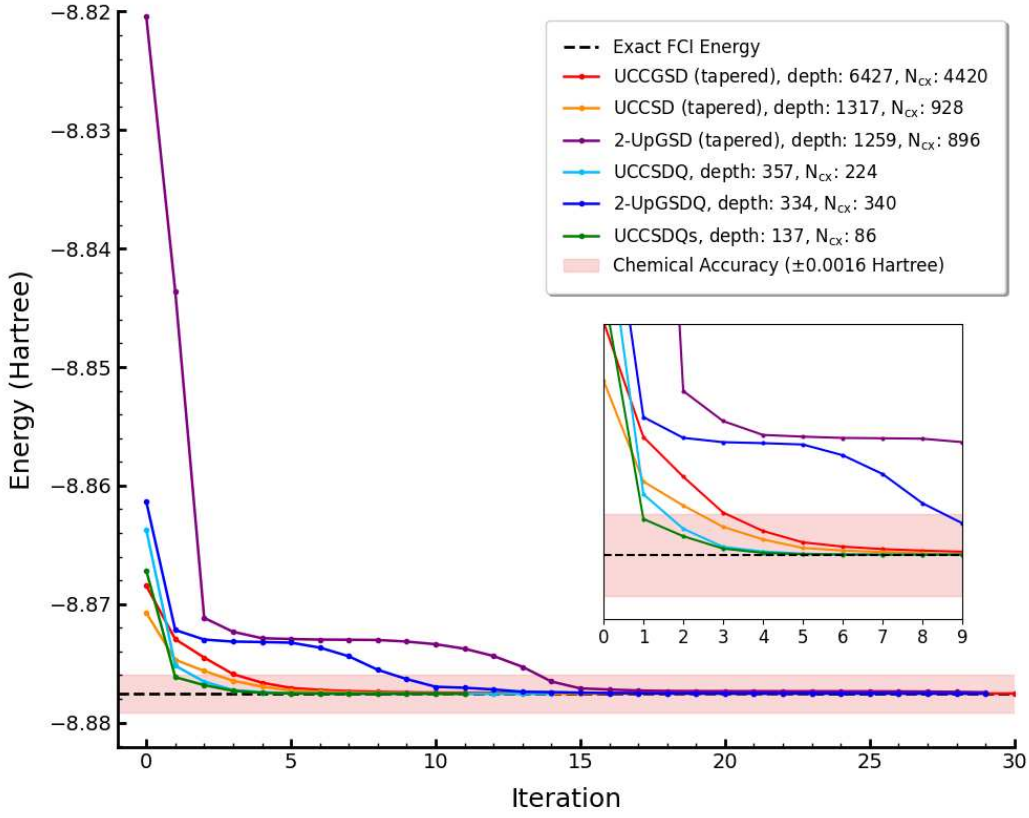

Figure 2. VQE calculation for the LiH molecule using various types of ansatzes and optimization methods. The plot compares the convergence of energy values with the FCI energy as a reference and indicates the chemical accuracy threshold, and N_{cx} represents the number of two-qubit gates. The inset illustrates convergence behavior during the first 10 optimization steps.

In Figure 3, we present the same analysis for the BeH_2 molecule. Again, one can see how the energy curve for each ansatz converges to the ground-state energy. The k-UpGSDQ ansatz requires four circuit repetitions to achieve convergence. As in the case of the LiH simulation, UCCSDQs proves to be the most resource-efficient, as it requires the fewest resources (circuit depth of 279 and a two-qubit gate count of 190) while staying within the

chemical accuracy range. The energy curves initially decrease rapidly, then stabilize as they approach the exact FCI value, highlighting the efficiency of these methods for BeH_2.

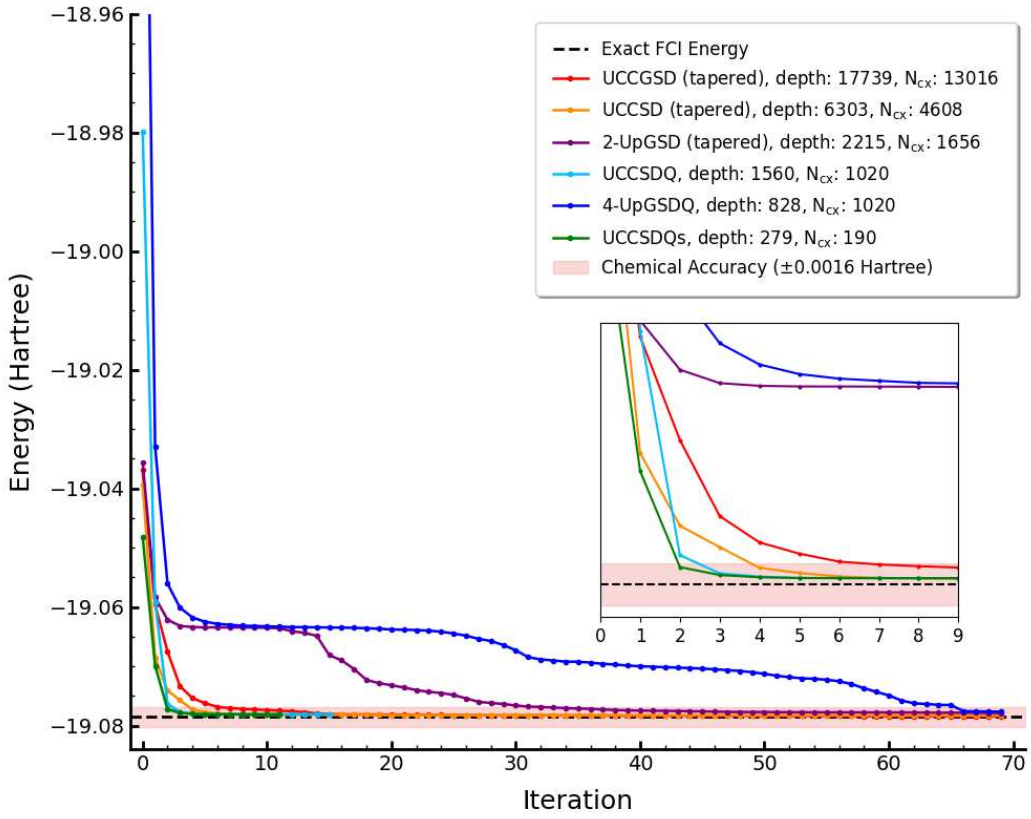

Figure 3. VQE calculation for the BeH_2 molecule using various types of ansatzes and optimization methods. The plot compares the convergence of energy values with the FCI energy as a reference and indicates the chemical accuracy threshold, and N_{cx} represents the number of two-qubit gates. The inset illustrates convergence behavior during the first 10 optimization steps.

We also simulate the methylamine molecule with a restricted number of spin orbitals. We take an active space of 6 electrons and 6 spin orbitals from the full 15-spin-orbital space and show the energy difference for this choice in Figure 4, which presents different active space configurations and their corresponding energies. This choice of active space allows us to reduce the number of qubits required to simulate the molecule down to 12. However, as seen in Figure 4, as the number of spin orbitals decreases, the calculated energy moves away from the reference coupled-cluster energy with single and double excitations (CCSD) and approaches the Hartree–Fock result. Chemical accuracy is achieved only when the core 1*s* orbitals are frozen. For the (6e, 6o) active space configuration of methylamine, we use the UCCSDQ and UCCSDQs ansatzes in the VQE calculation and the same minimal-basis STO-3G. As shown in Figure 5, the energy converges to the restricted active-space FCI value for both ansatzes. This result demonstrates that for the 12-qubit methylamine active space, the VQE algorithm, combined with the aforementioned ansatzes, can achieve chemical accuracy within a small number of iterations. Other types of ansatzes were not tested due to higher computational costs.

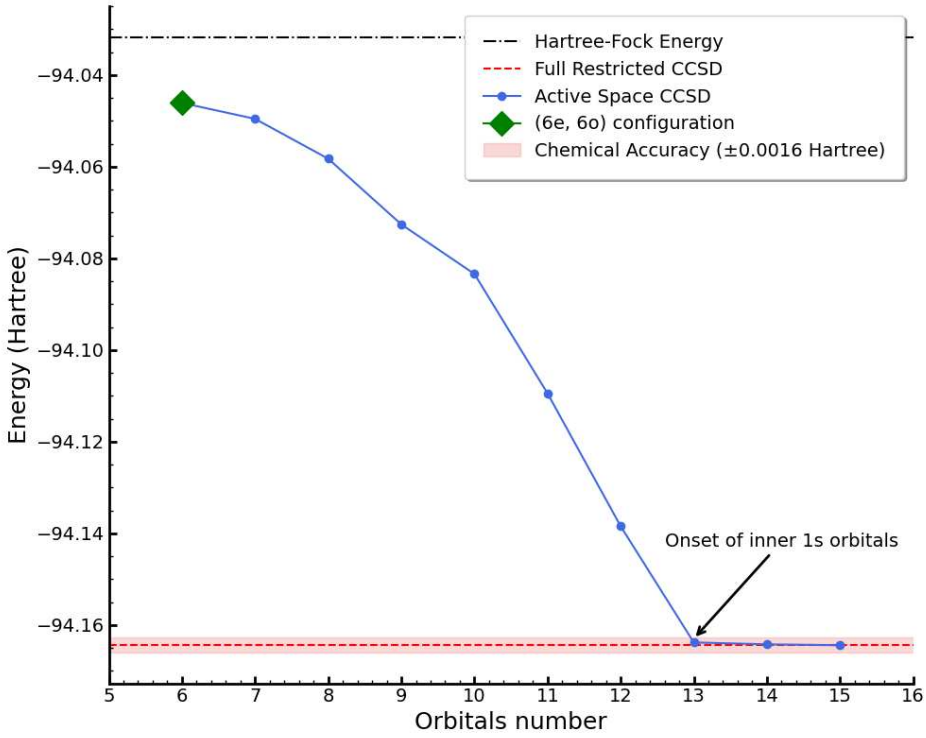

Figure 4. Ground-state energies for different active spaces of the methylamine molecule are shown. The green diamond marks the active space configuration used in the VQE calculation. The dash–dot black line indicates the Hartree–Fock energy, while the dashed red line corresponds to the restricted CCSD energy. The pink shaded region represents chemical accuracy around the CCSD reference. The black arrow points to the region where only the core (1*s*) orbitals are frozen.

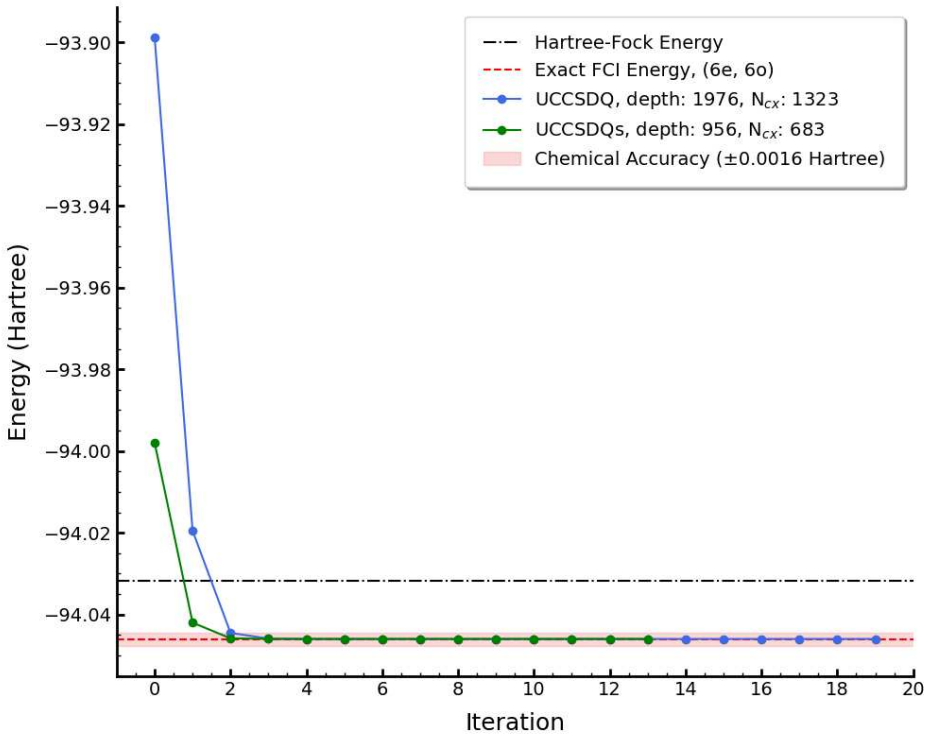

Figure 5. VQE calculation for the CH_3NH_2 molecule in (6e, 6o) active space using UCCSDQ and UCCSQs ansatzes. The black dash–dot line indicates the Hartree–Fock energy, while the dashed red line corresponds to the active-space FCI energy. The pink shaded region represents chemical accuracy around the FCI reference. N_{cx} represents the number of two-qubit gates.

Overall, these results show that the optimization strategies we use perform well for calculating ground-state energies of small molecules like LiH and BeH_2, as well as the methylamine molecule in reduced active space. They also highlight how different ansatz types can affect the balance between accuracy and resource needs. To better understand the origin of this performance and the trade-offs involved, we now turn to a more detailed discussion of convergence mechanisms and the behavior of different ansatz constructions.

6. Discussion

We begin our discussion with the choice of the k parameter in the k-UpGSD and k-UpGSDQ ansatzes, which directly affects both convergence and expressiveness. The value of k is chosen heuristically for each molecule by incrementally increasing k until the algorithm converges to the correct energy. The 1-UpGSD configuration has multiple nonphysical local minima due to the absence of orbital invariance in the pCCD-based (paired) double excitations [53]. Hence, with each additional exponential factor (see Equation (6)), one introduces an independent set of variational amplitudes. Consequently, the ansatz becomes more flexible and can capture more correlation effects, as observed in our simulations for LiH and BeH_2.

Another strategy demonstrating strong performance combines qubit excitations with irreducible representation filtering. There are several reasons why this combination performs better than other optimization strategies. First, the irreducible representation filtering removes excitations that do not coincide with the irreducible representation of the ground state. This decrease in the variational space dimensionality and the energy landscape becomes more simple: it has fewer local minima. Second, in conventional UCCSD, each fermionic excitation includes a string of Z operators to enforce anti-commutation, which introduces complex phase relationships into the circuit. While this makes the ansatz more physically accurate, it also tends to complicate the energy landscape locally. In contrast, qubit excitations avoid these phase strings, acting more like localized Pauli exponentials, which can lead to steeper initial gradients and faster energy reduction in early VQE iterations—a behavior similarly observed in the k-UpGSDQ ansatz.

However, scaling these optimization strategies to larger molecules represents a significantly greater challenge. Indeed, as shown in Table 2, the computational demands become significant. Even with the STO-3G minimal-basis set, the required circuit depth and the number of qubits for these molecules are far beyond what current quantum hardware can efficiently handle. The use of more complex bases that provide a better description of valence orbitals or account for polarization effects and electron correlations in molecules, such as 6-31G, 6-31G*, or cc-pVDZ, is associated with similar difficulties. All of them imply that significantly more qubits are required compared to the minimal-basis case. For instance, simulating the H_4 molecule using the cc-pVDZ basis would require 40 qubits [57]. To simulate the H_2O molecule in the 6-31g basis, 50 qubits are needed. For methylamine and formic acid molecules, the number of qubits exceeds 60. Recent studies [58,59] have investigated various ways to enable the simulation of relatively large systems with limited computational resources. A commonly used approach in these works is highest occupied molecular orbital–lowest unoccupied molecular orbital (HOMO-LUMO) approximation, which restricts the active space to a subset of orbitals of a molecule, as we do in the case of methylamine. This method results in a more compact qubit representation of the molecular system, making simulations more feasible. However, this reduction in active space introduces additional approximation errors, which can impact accuracy, as shown in Figure 4.

The VQE calculation for the formic acid molecule in a reduced active space, similar to the one performed for methylamine, does not converge well to the expected ground-state

energy. The explanation likely resides in stronger electronic correlations between carbon and oxygen atoms in the formic acid molecule, which cannot be adequately captured by circuits based on qubit excitations. It is possible that effective fermionic excitation circuits, as proposed in Ref. [50], could achieve better performance. Nevertheless, this comes at the cost of an increased two-qubit gate count. As a possible direction for future work, adaptive VQE methods could be explored using our UCCSDQs operator pool and compared with the minimal complete pool used in Ref. [16].

Moreover, all our optimization strategies include double excitation operators, which means they could face a fundamental challenge with barren plateaus under random parameter initialization and for a sufficiently large system size. As recent theoretical results indicate [60], once a variational ansatz includes two-body or generalized excitations, the expressiveness grows but may induce exponential gradient concentration. Empirically, one checks this by monitoring gradient variance over random initializations—exponential decay with the number of qubits signifies a barren plateau. This represents another potential direction for future research into the UCCSDQs ansatz types. Combining UCCSDQs with the qubit tapering procedure may offer additional resource savings; however, it requires a more careful analysis of the connection between $\mathbb{Z}_2$ symmetries and the representation of the excitation operator circuits.

Finally, we should emphasize the importance of testing our optimization strategies in error-prone simulations. We expect that a reduced circuit depth and fewer variational parameters will lead to significant improvements in optimization results.

7. Conclusions

In this study, we analyzed the computational resources required for VQE when modeling organic molecules such as formic acid and methylamine under various optimization strategies. Our goal was to identify how best to reduce circuit depth and gate counts while maintaining high accuracy in capturing electron correlation.

By implementing and testing different ansatzes, including qubit excitations filtered by irreducible representations (UCCSDQs), we demonstrated a significant reduction in the number of two-qubit gates required. This optimization allows us to recover most of the correlation energy while using fewer quantum resources, which is especially important, since low two-qubit gate fidelity is still a major limitation of current quantum devices.

Our resource estimates for full valence active-space simulations in molecules like methylamine and formic acid confirm that UCCSDQs achieves a favorable balance between circuit depth and algorithmic convergence. Nevertheless, real-world implementations still face hardware-level limitations, especially with respect to gate noise and qubit coherence times. To make VQE useful for real-world chemistry, we still need better ansatzes, more reliable quantum gates, and stronger error correction. We believe our work can support future research and help bring theoretical methods closer to today's quantum computers.

Author Contributions: Conceptualization, K.M.M. and A.K.F.; Methodology, K.M.M.; Software, K.M.M.; Validation, A.K.F.; Investigation, K.M.M.; Data curation, A.K.F.; Writing—original draft, K.M.M.; Writing—review and editing, A.K.F.; Visualization, K.M.M.; Supervision, A.K.F. All authors have read and agreed to the published version of the manuscript.

Funding: This research was funded by the Priority 2030 program at the NIST "MISIS" under project K1-2022-027.

Data Availability Statement: The data supporting the findings of this study are available from the corresponding authors upon reasonable request.

Conflicts of Interest: Owing to the employment and consulting activities of K.M.M. and A.K.F., they have financial interests in commercial applications of quantum computing.

References

1. Helgaker, T.; Jørgensen, P.; Olsen, J. *Molecular Electronic-Structure Theory*; Wiley: Hoboken, NJ, USA, 2000. [CrossRef]
2. Kempe, J.; Kitaev, A.; Regev, O. The Complexity of the Local Hamiltonian Problem. *SIAM J. Comput.* **2006**, *35*, 1070–1097. [CrossRef]
3. van Gunsteren, W.F.; Oostenbrink, C. Methods for Classical-Mechanical Molecular Simulation in Chemistry: Achievements, Limitations, Perspectives. *J. Chem. Inf. Model.* **2024**, *64*, 6281–6304. [CrossRef] [PubMed]
4. Lloyd, S. Universal Quantum Simulators. *Science* **1996**, *273*, 1073–1078. [CrossRef] [PubMed]
5. Cao, Y.; Romero, J.; Olson, J.P.; Degroote, M.; Johnson, P.D.; Kieferová, M.; Kivlichan, I.D.; Menke, T.; Peropadre, B.; Sawaya, N.P.D.; et al. Quantum Chemistry in the Age of Quantum Computing. *Chem. Rev.* **2019**, *119*, 10856–10915. [CrossRef]
6. McArdle, S.; Endo, S.; Aspuru-Guzik, A.; Benjamin, S.C.; Yuan, X. Quantum computational chemistry. *Rev. Mod. Phys.* **2020**, *92*, 015003. [CrossRef]
7. Fedorov, D.A.; Peng, B.; Govind, N.; Alexeev, Y. VQE method: A short survey and recent developments. *Mater. Theory* **2022**, *6*, 2. [CrossRef]
8. Huh, J.; Guerreschi, G.G.; Peropadre, B.; McClean, J.R.; Aspuru-Guzik, A. Boson sampling for molecular vibronic spectra. *Nat. Photonics* **2015**, *9*, 615–620. [CrossRef]
9. Argüello-Luengo, J.; González-Tudela, A.; Shi, T.; Zoller, P.; Cirac, J.I. Analogue quantum chemistry simulation. *Nature* **2019**, *574*, 215–218. [CrossRef]
10. Streif, M.; Neukart, F.; Leib, M. Solving Quantum Chemistry Problems with a D-Wave Quantum Annealer. In *Quantum Technology and Optimization Problems*; Feld, S., Linnhoff-Popien, C., Eds.; Springer International Publishing: Cham, Swizerland, 2019; pp. 111–122.
11. Xia, R.; Bian, T.; Kais, S. Electronic Structure Calculations and the Ising Hamiltonian. *J. Phys. Chem. B* **2018**, *122*, 3384–3395. [CrossRef]
12. Chermoshentsev, D.A.; Malyshev, A.O.; Esencan, M.; Tiunov, E.S.; Mendoza, D.; Aspuru-Guzik, A.; Fedorov, A.K.; Lvovsky, A.I. Polynomial unconstrained binary optimisation inspired by optical simulation. *arXiv* **2022**, arXiv:2106.13167.
13. Peruzzo, A.; McClean, J.; Shadbolt, P.; Yung, M.H.; Zhou, X.Q.; Love, P.J.; Aspuru-Guzik, A.; O'Brien, J.L. A variational eigenvalue solver on a photonic quantum processor. *Nat. Commun.* **2014**, *5*, 4213. [CrossRef] [PubMed]
14. McClean, J.R.; Romero, J.; Babbush, R.; Aspuru-Guzik, A. The theory of variational hybrid quantum-classical algorithms. *New J. Phys.* **2016**, *18*, 023023. [CrossRef]
15. Cerezo, M.; Arrasmith, A.; Babbush, R.; Benjamin, S.C.; Endo, S.; Fujii, K.; McClean, J.R.; Mitarai, K.; Yuan, X.; Cincio, L.; et al. Variational quantum algorithms. *Nat. Rev. Phys.* **2021**, *3*, 625–644. [CrossRef]
16. Sapova, M.; Fedorov, A. Variational quantum eigensolver techniques for simulating carbon monoxide oxidation. *Commun. Phys.* **2022**, *5*, 199. [CrossRef]
17. Tilly, J.; Chen, H.; Cao, S.; Picozzi, D.; Setia, K.; Li, Y.; Grant, E.; Wossnig, L.; Rungger, I.; Booth, G.H.; et al. The Variational Quantum Eigensolver: A review of methods and best practices. *Phys. Rep.* **2022**, *986*, 1–128. [CrossRef]
18. Kandala, A.; Mezzacapo, A.; Temme, K.; Takita, M.; Brink, M.; Chow, J.M.; Gambetta, J.M. Hardware-efficient variational quantum eigensolver for small molecules and quantum magnets. *Nature* **2017**, *549*, 242–246. [CrossRef] [PubMed]
19. Powell, M.J. A trust-region algorithm for optimization without derivatives. *Math. Program.* **2003**, *97*, 605–623. [CrossRef]
20. Bravyi, S.; Sheldon, S.; Kandala, A.; Mckay, D.C.; Gambetta, J.M. Scalable mitigation of measurement errors on quantum computers. *PRX Quantum* **2021**, *2*, 040326. [CrossRef]
21. O'Malley, P.J.J.; Babbush, R.; Kivlichan, I.D.; Romero, J.; McClean, J.R.; Barends, R.; Kelly, J.; Roushan, P.; Tranter, A.; Ding, N.; et al. Scalable Quantum Simulation of Molecular Energies. *Phys. Rev. X* **2016**, *6*, 031007. [CrossRef]
22. Hempel, C.; Maier, C.; Romero, J.; McClean, J.; Monz, T.; Shen, H.; Jurcevic, P.; Lanyon, B.P.; Love, P.; Babbush, R.; et al. Quantum Chemistry Calculations on a Trapped-Ion Quantum Simulator. *Phys. Rev. X* **2018**, *8*, 031022. [CrossRef]
23. Nam, Y.; Chen, J.S.; Pisenti, N.C.; Wright, K.; Delaney, C.; Maslov, D.; Brown, K.R.; Allen, S.; Amini, J.M.; Apisdorf, J.; et al. Ground-state energy estimation of the water molecule on a trapped-ion quantum computer. *Npj Quantum Inf.* **2020**, *6*, 33. [CrossRef]
24. Arute, F.; Arya, K.; Babbush, R.; Bacon, D.; Bardin, J.C.; Barends, R.; Boixo, S.; Broughton, M.; Buckley, B.B.; Buell, D.A.; et al. Hartree-Fock on a superconducting qubit quantum computer. *Science* **2020**, *369*, 1084–1089. [CrossRef]
25. Bentellis, A.; Matic-Flierl, A.; Mendl, C.B.; Lorenz, J.M. Benchmarking the Variational Quantum Eigensolver using different quantum hardware. In Proceedings of the 2023 IEEE International Conference on Quantum Computing and Engineering (QCE), Bellevue, DC, USA, 1–4 October 2023; Volume 1, pp. 518–523.
26. Hu, J.; Li, J.; Lin, Y.; Long, H.; Xu, X.S.; Su, Z.; Zhang, W.; Zhu, Y.; Yung, M.H. Benchmarking variational quantum eigensolvers for quantum chemistry. *arXiv* **2022**, arXiv:2211.12775.
27. Singh, H.; Majumder, S.; Mishra, S. SHARC-VQE: Simplified Hamiltonian Approach with Refinement and Correction enabled Variational Quantum Eigensolver for Molecular Simulation. *arXiv* **2024**, arXiv:2407.12305. [CrossRef]

28. Makushin, K.; Baibekov, E. Quantum computation of the lowest-energy Kramers states and magnetic g-factors of rare earth ions in crystals. *Magn. Reson. Solids* **2023**, *25*, 23204. [CrossRef]
29. Steiger, D.S.; Häner, T.; Genin, S.N.; Katzgraber, H.G. Sparse Simulation of VQE Circuits for Quantum Chemistry. *arXiv* **2024**, arXiv:2404.10047.
30. Rocca, D.; Cortes, C.L.; Gonthier, J.F.; Ollitrault, P.J.; Parrish, R.M.; Anselmetti, G.L.; Degroote, M.; Moll, N.; Santagati, R.; Streif, M. Reducing the runtime of fault-tolerant quantum simulations in chemistry through symmetry-compressed double factorization. *J. Chem. Theory Comput.* **2024**, 24, 4639–4653. [CrossRef] [PubMed]
31. Shang, H.; Shen, L.; Fan, Y.; Xu, Z.; Guo, C.; Liu, J.; Zhou, W.; Ma, H.; Lin, R.; Yang, Y.; et al. Large-scale simulation of quantum computational chemistry on a new sunway supercomputer. In Proceedings of the SC22: International Conference for High Performance Computing, Networking, Storage and Analysis, Dallas, TX, USA, 13–18 November 2022.
32. Zhou, L.; Wang, S.-T.; Choi, S.; Pichler, H.; Lukin, M.D. Quantum Approximate Optimization algorithm: Performance, Mechanism, and Implementation on Near-Term Devices. *Phys. Rev. X* **2020**, *10*, 021067. [CrossRef]
33. Sun, Z.-H.; Wang, Y.-Y.; Cui, J.; Fan, H. Improving the performance of quantum approximate optimization for preparing non-trivial quantum states without translational symmetry. *New J. Phys.* **2023**, *25*, 013015. [CrossRef]
34. Matos, G.; Self, C.N.; Papić, Z.; Meichanetzidis, K.; Dreyer, H. Characterization of variational quantum algorithms using free fermions. *Quantum* **2023**, *7*, 966. [CrossRef]
35. Kaubruegger, R.; Silvi, P.; Kokail, C.; van Bijnen, R.; Rey, A.M.; Ye, J.; Kaufman, A.M.; Zoller, P. Variational Spin-Squeezing Algorithms on Programmable Quantum Sensors. *Phys. Rev. Lett.* **2019**, *123*, 260505. [CrossRef] [PubMed]
36. Sun, Z.-H.; Wang, Y.-Y.; Zhang, Y.-R.; Nori, F.; Fan, H. Variational generation of spin squeezing on one-dimensional quantum devices with nearest-neighbor interactions. *Phys. Rev. Res.* **2023**, *5*, 043285. [CrossRef]
37. Santra, G.C.; Jendrzejewski, F.; Hauke, P.; Egger, D.J. Squeezing and quantum approximate optimization. *Phys. Rev. A* **2024**, *109*, 012413. [CrossRef]
38. Zhang, J.; Li, Y.; Li, Q.; Xiao, W. Variance-constrained local–global modeling for device-free localization under uncertainties. *IEEE Trans. Ind. Inform.* **2024**, *20*, 5229–5240. [CrossRef]
39. Zhang, J.; Xue, J.; Li, Y.; Cotton, S.L. Leveraging online learning for domain-adaptation in Wi-Fi-based device-free localization. *IEEE Trans. Mob. Comput.* **2025**, *01*, 1–15. [CrossRef]
40. Carleo, G.; Troyer, M. Solving the quantum many-body problem with artificial neural networks. *Science* **2017**, *355*, 602–606. [CrossRef]
41. Pfau, D.; Spencer, J.S.; Matthews, A.G.d.G.; Foulkes, W.M.C. Ab initio solution of the many-electron Schrödinger equation with deep neural networks. *Phys. Rev. Res.* **2020**, *2*, 033429. [CrossRef]
42. Hermann, J.; Schätzle, Z.; Noé, F. Deep neural network solution of the electronic Schrödinger equation. *Nat. Chem.* **2020**, *12*, 891–897. [CrossRef]
43. Grimsley, H.; Economou, S.; Barnes, E.; Mayhall, N.J. An adaptive variational algorithm for exact molecular simulations on a quantum computer. *Nat. Commun.* **2019**, *10*, 3007. [CrossRef]
44. Chivilikhin, D.; Samarin, A.; Ulyantsev, V.; Iorsh, I.; Oganov, R.; Kyriienko, O. MoG-VQE: Multiobjective genetic variational quantum eigensolver. *arXiv* **2020**, arXiv:2007.04424.
45. Wu, Y.; Jiang, Z.; Lin, Z.; Liang, Y.; Wang, H. Direct electrosynthesis of methylamine from carbon dioxide and nitrate. *Nat. Sustain.* **2021**, *4*, 1–6. [CrossRef]
46. Fedorov, A.K.; Gelfand, M.S. Towards practical applications in quantum computational biology. *Nat. Comput. Sci.* **2021**, *1*, 114–119. [CrossRef]
47. Bravyi, S.; Gambetta, J.; Mezzacapo, A.; Temme, K. Tapering off qubits to simulate fermionic Hamiltonians. *arXiv* **2017**, arXiv:1701.08213.
48. NIST Computational Chemistry Comparison and Benchmark Database. NIST Standard Reference Database Number 101, Release 22, 2022. Available online: http://cccbdb.nist.gov/ (accessed on 5 February 2025).
49. Gokhale, P.; Angiuli, O.; Ding, Y.; Gui, K.; Tomesh, T.; Suchara, M.; Martonosi, M.; Chong, F.T. Optimization of simultaneous measurement for variational quantum eigensolver applications. In Proceedings of the 2020 IEEE International Conference on Quantum Computing and Engineering (QCE), Broomfield, CO, USA, 12–16 October 2020; pp. 379–390.
50. Yordanov, Y.S.; Arvidsson-Shukur, D.R.; Barnes, C.H. Efficient quantum circuits for quantum computational chemistry. *Phys. Rev. A* **2020**, *102*, 062612. [CrossRef]
51. Yordanov, Y.S.; Armaos, V.; Barnes, C.H.; Arvidsson-Shukur, D.R. Qubit-excitation-based adaptive variational quantum eigensolver. *Commun. Phys.* **2021**, *4*, 228. [CrossRef]
52. Magoulas, I.; Evangelista, F.A. Linear-scaling quantum circuits for computational chemistry. *J. Chem. Theory Comput.* **2023**, *19*, 4815–4821. [CrossRef] [PubMed]
53. Lee, J.; Huggins, W.J.; Head-Gordon, M.; Whaley, K.B. Generalized Unitary Coupled Cluster Wave Functions for Quantum Computation. *J. Chem. Theory Comput.* **2018**, *15*, 311–324. [CrossRef]

54. Burton, H.G.; Marti-Dafcik, D.; Tew, D.P.; Wales, D.J. Exact electronic states with shallow quantum circuits from global optimisation. *Npj Quantum Inf.* **2023**, *9*, 75. [CrossRef]
55. Cao, C.; Hu, J.; Zhang, W.; Xu, X.; Chen, D.; Yu, F.; Li, J.; Hu, H.S.; Lv, D.; Yung, M.H. Progress toward larger molecular simulation on a quantum computer: Simulating a system with up to 28 qubits accelerated by point-group symmetry. *Phys. Rev. A* **2022**, *105*, 062452. [CrossRef]
56. Makushin, K.; Sapova, M.; Fedorov, A. Quantum computing library for quantum chemistry applications. In *Journal of Physics: Conference Series*; IOP Publishing: Bristol, UK, 2024; Volume 2701, p. 012032.
57. Guo, C.; Fan, Y.; Xu, Z.; Shang, H. Differentiable matrix product states for simulating variational quantum computational chemistry. *Quantum* **2023**, *7*, 1192. [CrossRef]
58. Li, W.; Huang, Z.; Cao, C.; Huang, Y.; Shuai, Z.; Sun, X.; Sun, J.; Yuan, X.; Lv, D. Toward practical quantum embedding simulation of realistic chemical systems on near-term quantum computers. *Chem. Sci.* **2022**, *13*, 8953–8962. [CrossRef] [PubMed]
59. Shang, H.; Fan, Y.; Shen, L., Guo, C.; Liu, J.; Duan, X.; Li, F.; Li, Z. Towards practical and massively parallel quantum computing emulation for quantum chemistry. *Npj Quantum Inf.* **2023**, *9*, 33. [CrossRef] [PubMed]
60. Mao, R.; Tian, G.; Sun, X. Towards determining the presence of barren plateaus in some chemically inspired variational quantum algorithms. *Commun. Phys.* **2024**, *7*, 342. [CrossRef]